J|A|C|S
ARTICLES
Published on Web 02/16/2005

Heme/Non-Heme Diiron(II) Complexes and O_2, CO, and NO Adducts as Reduced and Substrate-Bound Models for the Active Site of Bacterial Nitric Oxide Reductase

Ian M. Wasser,[†] Hong-wei Huang,[‡] Pierre Moënne-Loccoz,[‡] and Kenneth D. Karlin*[,†]

Contribution from the Department of Chemistry, Johns Hopkins University, Charles and 34th Streets, Baltimore, Maryland 21218, and Department of Environmental & Biomolecular Systems, OGI School of Science & Engineering, Oregon Health & Science University, Beaverton, Oregon 97006

Received July 9, 2004; E-mail: karlin@jhu.edu

Abstract: As a first generation model for the reactive reduced active-site form of bacterial nitric oxide reductase, a heme/non-heme diiron(II) complex $[(^6L)Fe^{II}\cdots Fe^{II}-(Cl)]^+$ (**2**) {where ^6L = partially fluorinated tetraphenylporphyrin with a tethered tetradentate TMPA chelate; TMPA = tris(2-pyridyl)amine} was generated by reduction of the corresponding μ-oxo diferric compound $[(^6L)Fe^{III}-O-Fe^{III}-Cl]^+$ (**1**). Coordination chemistry models for reactions of reduced NOR with O_2, CO, and NO were also developed. With O_2 and CO, adducts are formed, $[(^6L)Fe^{III}(O_2^-)(thf)\cdots Fe^{II}-Cl]B(C_6F_5)_4$ (**2a**·O_2) {λ_{max} 418 (Soret), 536 nm; $\nu_{O-O} = 1176$ cm^{-1}, $\nu_{Fe-O} = 574$ cm^{-1} and $[(^6L)Fe^{II}(CO)(thf)Fe^{II}-Cl]B(C_6F_5)_4$ (**2a**·CO) {ν_{CO} 1969 cm^{-1}}, respectively. Reaction of purified nitric oxide with **2** leads to the dinitrosyl complex $[(^6L)Fe(NO)Fe(NO)-Cl]B(C_6F_5)_4$ (**2a**·$(NO)_2$) with ν_{NO} absorptions at 1798 cm^{-1} (non-heme Fe−NO) and 1689 cm^{-1} (heme−NO).

Introduction

Bacterial denitrification is the anaerobic alternative to aerobic respiration or photosysnthesis, in which nitrogen oxides are used as terminal electron acceptors.[1,2] The four reductive steps (see below) in this cycle are catalyzed by metalloenzymes. In these regards, considerable efforts are being devoted to understanding the interactions of metalloproteins and/or relevant coordination compounds with nitrogen oxides.[2−7]

$$NO_3^- \rightarrow NO_2^- \rightarrow NO \rightarrow N_2O \rightarrow N_2 \qquad (1)$$

Nitric oxide reductase (NOR) is a membrane-bound bacterial enzyme that catalyzes the third step (eq 1), the reduction of nitric oxide to nitrous oxide, using electrons donated from soluble cytochrome *c*.[2,3,8,9] NOR isolated from *Paracoccus denitrificans* has been shown to contain one high-spin and one low-spin heme *b*, one low-spin heme *c*, and a non-heme iron (Fe_B) per enzyme (Figure 1).[10−13] The Fe_B is coordinated by nitrogen atoms from three histidine ligands with possible ligation by an additional glutamate residue. The NorB subunit, which includes the diiron active site, exhibits *weak* homology to subunit I of cytochrome *c* oxidase (C*c*O), which couples the reduction of O_2 to water with membrane proton translocation; the six histidine residues that ligate heme *a*, heme a_3, and Cu_B in C*c*O are conserved in NOR.[14,15] In essence, the Cu_B site of C*c*O has been replaced by a non-heme iron (Fe_B) in NOR; C*c*O and NOR are genetic cousins.[1,2,12,13,16]

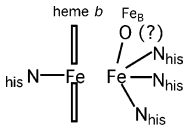

Figure 1. Schematic representation of the NOR active site showing the binuclear center where NO(g) reductive coupling occurs, producing nitrous oxide (N_2O).

Our own interest in this area stems from the examination of heme/copper oxidase model complexes and their interactions with dioxygen, relevant to the heme a_3/Cu_B binuclear active site in C*c*O.[17−21] One iron/copper system studied employs a binucleating ligand (e.g., ^6L; Chart 1) {^6L is the dianion of

[†] Johns Hopkins University.
[‡] Oregon Health & Science University.

(1) Zumft, W. G. *Microbiol. Mol. Biol. Rev.* **1997**, *61*, 533−616.
(2) Wasser, I. M.; de Vries, S.; Moënne-Loccoz, P.; Schröeder, I.; Karlin, K. D. *Chem. Rev.* **2002**, *102*, 1201−1234.
(3) Averill, B. A. *Chem. Rev.* **1996**, *96*, 2951−2964.
(4) Ford, P. C.; Lorkovic, I. *Chem. Rev.* **2002**, *102*, 993−1017.
(5) Coppens, P.; Novozhilova, I.; Kovalevsky, A. *Chem. Rev.* **2002**, *102*, 861−884.
(6) Butler, A.; Megson, I. L. *Chem. Rev.* **2002**, *102*, 1155−1166.
(7) McCleverty, J. A. *Chem. Rev.* **2004**, *104*, 403−418.
(8) Moura, I.; Moura, J. J. G. *Curr. Opin. Chem. Biol.* **2001**, *5*, 168−175.
(9) Richardson, D. J.; Watmough, N. J. *Curr. Opin. Chem. Biol.* **1999**, *3*, 207−19.
(10) Hendriks, J. H. M.; Gohlke, U.; Saraste, M. *J. Bioenergetics Biomembranes* **1998**, *30*, 15−24.
(11) Hendriks, J. W. A.; Gohlke, U.; Haltia, T.; Ludovici, C.; Lubben, M.; Saraste, M. *Biochemistry* **1998**, *37*, 13102−13109.
(12) Girsch, P.; de Vries, S. *Biochim. Biophys. Acta* **1997**, *1318*, 202−216.
(13) Moënne-Loccoz, P.; de Vries, S. *J. Am. Chem. Soc.* **1998**, *120*, 5147.
(14) de Vries, S.; Schröeder, I. *Biochem. Soc. Trans.* **2002**, *30*, 662−667.
(15) Saraste, M.; Castresana, J. *FEBS Lett.* **1994**, *341*, 1−4.
(16) Pinakoulaki, E.; Gemeinhardt, S.; Saraste, M.; Varostis, C. *J. Biol. Chem.* **2002**, *277*, 23407−23413.

10.1021/ja0458773 CCC: $30.25

Chart 1

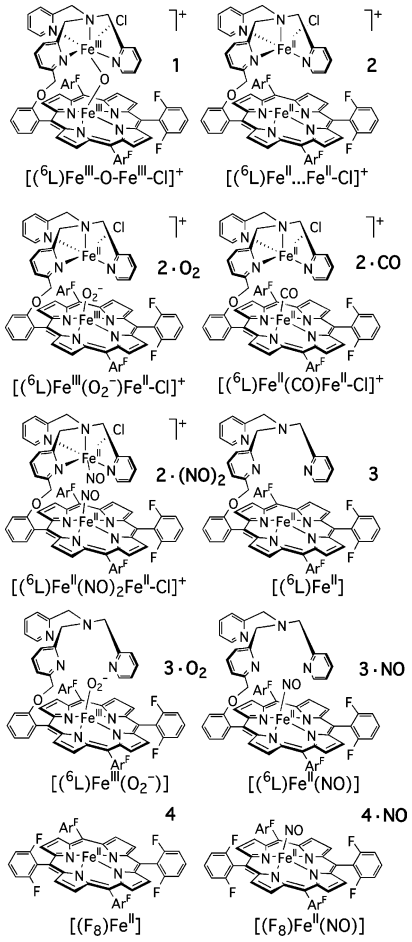

5-(*ortho*-*O*-[(*N*,*N*-bis(2-pyridylmethyl)-2-(6-methoxyl)pyridine-methanamine)phenyl]-10,15,20-tris(2,6-difluorophenyl)porphine} featuring a porphyrin tethered to a tetradentate chelate (TMPA, tris(2-pyridylmethyl)amine) able to coordinate copper.[17] Given the similarities between the active sites in C*c*O and NOR, an obvious extension would be to incorporate a non-heme iron ion at the TMPA tether, which we have previously accomplished in investigations featuring "resting" or oxidized active site NOR models.[22−25]

Thus, our previous efforts have included the synthesis of several μ-oxo heme/non-heme diiron compounds.[23,25] There has also been a cursory examination of the reactivity of one reduced heme/non-heme diiron complex with dioxygen and nitric oxide.[24] Here, we report the synthesis and characterization of the complex $[(^6L)Fe^{II}\cdots Fe^{II}-Cl]^+$ (**2**), a reduced heme/non-heme diiron complex, representing a spectroscopic and/or structural model for the putative active (reduced) site in NOR. Furthermore, we have examined the reactivity of **2** with dioxygen, carbon monoxide, and nitric oxide, as it is important to lay the foundation for understanding the interactions and basic coordination chemistry of these small molecules in a heme/non-heme diiron(II) environment. Bacterial NOR has been found to reduce dioxygen in a manner similar to C*c*O (i.e., having oxidase activity),[26,27] while CO often serves as an O_2 or NO surrogate or probe for spectroscopic and structural studies of biologically relevant iron enzymes or complexes.[28−38] A detailed examination of the dioxygen reactivity of $[(^6L)Fe^{II}\cdots Fe^{II}-Cl]B(C_6F_5)_4$ (**2a**) provides proof that this dioxygen adduct is $[(^6L)Fe^{III}(O_2^-)\cdots Fe^{II}-Cl]B(C_6F_5)_4$ (**2a**·O_2), a superoxo rather than a peroxo species (Chart 1). We have further examined the formation of the heme−dioxygen (superoxo) complex in a closely related "empty tether" complex, the reaction of $[(^6L)Fe^{II}]$ (**3**) + O_2 producing $[(^6L)Fe^{III}(O_2^-)]$ (**3**·O_2) (Chart 1). Finally, we present the first substrate bound (e.g., NO and analogue CO) model complexes for NOR, room-temperature stable monocarbonyl (**2a**·CO), and dinitrosyl (**2a**·$(NO)_2$) adducts. The characterization includes vibrational studies of the related nitrosyl compounds formed from reactions of $[(^6L)Fe^{II}]$ (**3**) or $[(F_8)Fe^{II}]$ (**4**) and NO(g). We find that complexes **4** and **4**·NO do not catalyze the disproportionation of NO(g).

Experimental Section

Materials and Methods. Reagents were obtained from commercial sources. Dichloromethane (CH_2Cl_2), tetrahydrofuran (THF), and toluene were purified and dried by passing reagent-grade solvent through a series of two activated alumina columns. Acetone was dried over and then distilled from indicator-free calcium sulfate. Deoxygenation of these solvents was performed by bubbling with argon for 20 min followed by three freeze/pump/thaw cycles. Deuterated tetrahydrofuran (THF-d_8) was distilled from a sodium/benzophenone ketyl and degassed by three freeze/pump/thaw cycles. Using the modified procedures based on the methods of Ford and co-workers,[4] nitric oxide (research grade/BOC gases) was purified by passage through a series of two Ascarite II columns and finally distilled at 173 K. ^{15}NO (99%, ICON isotopes, Summit, NJ) was distilled at 173 K prior to use. Carbon monoxide (Matheson Gas Products) was purified by passage through an R & D Separations oxygen/moisture trap (model OT3-4). Bulbs of $^{18}O_2$ (99%,

(17) Ghiladi, R. A.; Ju, T. D.; Lee, D.-H.; Moënne-Loccoz, P.; Kaderli, S.; Neuhold, Y.-M.; Zuberbüehler, A. D.; Woods, A. S.; Cotter, R. J.; Karlin, K. D. *J. Am. Chem. Soc.* **1999**, *121*, 9885−9886.
(18) Ju, T. D.; Ghiladi, R. A.; Lee, D.-H.; van Strijdonck, G. P. F.; Woods, A. S.; Cotter, R. J.; Young, V. G., Jr.; Karlin, K. D. *Inorg. Chem.* **1999**, *38*, 2244−2245.
(19) Obias, H. V.; van Strijdonck, G. P. F.; Lee, D.-H.; Ralle, M.; Blackburn, N. J.; Karlin, K. D. *J. Am. Chem. Soc.* **1998**, *120*, 9696−9697.
(20) Kim, E.; Helton, M. E.; Wasser, I. M.; Karlin, K. D.; Lu, S.; Huang, H.-w.; Moenne-Loccoz, P.; Incarvito, C. D.; Rheingold, A. L.; Honecker, M.; Kaderli, S.; Zuberbuhler, A. D. *Proc. Natl. Acad. Sci. U.S.A.* **2003**, *100*, 3623−3628.
(21) Kim, E.; Chufan, E. E.; Kamaraj, K.; Karlin, K. D. *Chem. Rev.* **2004**, *104*, 1077−1133.
(22) Moënne-Loccoz, P.; Richter, O.-M. H.; Huang, H.-W.; Wasser, I. M.; Ghiladi, R. A.; Karlin, K. D.; de Vries, S. *J. Am. Chem. Soc.* **2000**, *122*, 9344−9345.
(23) Martens, C. F.; Murthy, N. N.; Obias, H. V.; Karlin, K. D. *J. Chem. Soc., Chem. Commun.* **1996**, 629−630.
(24) Ju, T. D.; Woods, A. S.; Cotter, R. J.; Moënne-Loccoz, P.; Karlin, K. D. *Inorg. Chim. Acta* **2000**, *297*, 362−372.
(25) Wasser, I. M.; Martens, C. F.; Verani, C. N.; Rentschler, E.; Huang, H.-w.; Moeenne-Loccoz, P.; Zakharov, L. N.; Rheingold, A. L.; Karlin, K. D. *Inorg. Chem.* **2004**, *43*, 651−662.
(26) Fujiwara, T.; Fukumori, Y. *J. Bacteriol.* **1996**, *178*, 1866−1871.
(27) Butland, G.; Spiro, S.; Watmough, N. J.; Richardson, D. J. *J. Bacteriol.* **2001**, *183*, 189−199.
(28) Spiro, T. G.; Zgierski, M. Z.; Kozlowski, P. M. *Coord. Chem. Rev.* **2001**, *219−221*, 923−936.
(29) Spiro, T. G.; Kozlowski, P. M. *Acc. Chem. Res.* **2001**, *34*, 137−144.
(30) Zhang, Y.; Palosky, M. A.; Brown, C. A.; Westre, T. E.; Hedman, B.; Hodgson, K. O.; Solomon, E. I. *J. Am. Chem. Soc.* **1992**, *114*, 9189−9191.
(31) Brown, C. A.; Palosky, M. A.; Westre, T. E.; Zhang, Y.; Hedman, B.; Hodgson, K. O.; Solomon, E. I. *J. Am. Chem. Soc.* **1995**, *117*, 715−732.
(32) Randall, C. R.; Zang, Y.; True, A. E.; Que, J. L.; Charnock, J. M.; Garner, C. D.; Fujishima, Y.; Schofield, C. J.; Baldwin, J. E. *Biochemistry* **1993**, *32*, 6664−6673.
(33) Que, J. L.; Dong, Y. *Acc. Chem. Res.* **1996**, *29*, 190−196.
(34) Que, J. L. *J. Chem. Soc., Dalton Trans.* **1997**, 3922−3940.
(35) Hsu, H.-F.; Yoo, S. J.; Münck, E.; Que, J. L. *J. Am. Chem. Soc.* **2000**, *122*, 3789−3790.
(36) MacMurdo, V. L.; Zheng, H.; Que, J. L. *Inorg. Chem.* **2000**, *39*, 2254−2255.
(37) Costas, M.; Chen, K.; Que, J. L. *Coord. Chem. Rev.* **2000**, *200−202*, 517−544.
(38) Kryatov, S. V.; Rybak-Akimova, E. V.; MacMurdo, V. L.; Que, J. L. *Inorg. Chem.* **2001**, *40*, 2220−2228.

ICON Isotopes, Summit, NJ) gas were held at 193 K prior to use. The preparation and handling of air-sensitive materials was carried out with Schlenk techniques under argon or in an MBraun Labmaster 130 glovebox held under nitrogen gas (O_2 < 1 ppm; H_2O < 1 ppm).

Elemental analyses were performed by Desert Analytics (Tucson, AZ) or Quantitative Technologies, Inc. (QTI, Whitehouse, NJ). ^{1}H NMR spectra were recorded at 300 MHz on a Bruker AMX-300 instrument. Chemical shifts are reported as δ values relative to an internal standard (Me_4Si) and the residual solvent proton peak. Infrared spectra were obtained on either a Mattson Galaxy 4030 FT-IR spectrometer or an in situ ReactIR 1000 FTIR spectrometer (RIR) with SiComp ATR probe tip (Mettler-Toledo, Millersville, MD). Solid samples were prepared by dissolving a sample in solution in the glovebox, spotting a CaF_2 IR window, and allowing the solvent to evaporate. Alternatively, IR measurements were made by evaporating solutions of a sample, under a stream of argon, onto a SiComp ATR probe window. Air-sensitive UV−visible samples were prepared in the glovebox in the appropriate deoxygenated solvent. Low-temperature UV−visible spectra were recorded with a Hewlett-Packard 8453 diode array spectrometer equipped with HPChemstation software. Low-temperature UV−visible spectra were recorded using a modified literature procedure.[39,40] Briefly, a quartz-windowed vacuum dewar was connected (via copper tubing) to a methanol-filled external recirculating cold bath (Neslab Endocal). The methanol temperature within the dewar was monitored using a thermocouple probe (Omega Model 651). The cuvette assembly consisted of a four-window quartz cuvette (1 cm path) connected, via a 12 cm glass tube, to a 14/20 female ground glass joint and a glass stopcock. Room-temperature UV−visible spectra were recorded with a Varian Cary-50 spectrophotometer. Electron paramagnetic resonance (EPR) spectra were obtained on a Bruker EMX spectrometer operating at X-band. Matrix-assisted laser desorption−ionization time-of-flight mass spectrometry (MALDI-MS) was performed using a Kratos Kompact 4 spectrometer and the porphyrin complexes were examined without added matrix. MALDI samples were prepared on stainless steal plates (20 well) in the glovebox and sealed in a long air-free reaction flask with a rubber septum. Once removed from the glovebox and positioned near the spectrometer, MALDI plates were quickly removed from the flask under a stream of dry argon and inserted into the instrument to minimize exposure to the ambient atmosphere.

Synthesis. [(^{6}L)Fe^{III}−O−Fe^{III}−Cl]B(C_6F_5)$_4$ (**1a**),[25] [(^{6}L)Fe^{III}−O−Fe^{III}−Cl]PF_6 (**1b**),[25] [(^{6}L)Fe^{II}] (**3**),[18,41] and [(F_8)Fe^{II}] (**4**)[42,43] were prepared as described in the literature.

[(^{6}L)Fe^{II}···Fe^{II}−Cl]B(C_6F_5)$_4$ (2a). Under argon, a solution of [(^{6}L)-Fe^{III}−O−Fe^{III}−Cl]B(C_6F_5)$_4$ (**1a**) (250 mg, 0.132 mmol) in deoxygenated CH_2Cl_2 (40 mL) was added to a 1 M solution of sodium dithionite in deoxygenated water (50 mL). The heterogeneous phases were mixed with vigorous argon bubbling for 35 min, at which time the organic layer had turned from a dark red to a bright red color. The solvent was removed and the crude material recrystallized from a THF and heptane mixture overnight at room temperature. The resulting microcrystalline material was filtered and dried under reduced pressure to yield a purple-red solid (200 mg, 81%). ^{1}H NMR (THF-d_8, 300 MHz): δ 91 (br, α-H), 82 (br, methylene −CH_2−), 59 (s, PY−H, β), 57 (s, PY−H, β), 50−47 (m, pyrrole-H), 46−44 (m, PY−H), 43−35 (m, PY−H), 21 (m, pyrrole-H), 7.9−7.2 (*m*- and *p*-phenyl-H), −6.1 (PY−H, γ), −7.5 (PY−H, γ), −19 (br, α-H). UV−Vis (THF; nm, ϵ mol^{-1} L^{-1}): 310, 23000; 424, 205000; 544, 9900. FTIR (film, cm^{-1}) 1644, 1625, 1606, 1583, 1513, 1463, 1413, 1374, 1336, 1274, 1235, 1204. MALDI-TOF-MS: *m*/*z* 1188 (M + 2H$^+$ − BArF$^-$)$^+$.

[(^{6}L)Fe^{II}···Fe^{II}−Cl]PF_6 (2b). A procedure, identical to the one employed for the synthesis of **2a**, was utilized with the exception that [(^{6}L)Fe^{III}−O−Fe^{III}−Cl]PF_6 (**1b**) was reduced. The resulting product is a bright red solid (192 mg, 80%). UV−Vis (THF; nm, ϵ mol^{-1} L^{-1}): 310, 23000; 424, 205000; 544, 9900. Anal. Calcd for $C_{67}H_{48}ClF_{12}Fe_2N_8O_2P$ (**2b**·C_4H_8O): C, 57.35; H, 3.45; N, 7.99. Found: C, 57.18; H, 3.43; N, 8.17.

[(^{6}L)Fe^{III}(O_2^-)···Fe^{II}−Cl]B(C_6F_5)$_4$ (2a·O_2). UV−visible scale samples were prepared using a THF solution (5×10^{-5} M) of **2a** in an air-free cuvette assembly fitted with a rubber septum. Subsquent cooling to 193 K was followed by the gentle bubbling with dioxygen via syring needle. Samples of **2a**·O_2 were prepared for RR spectroscopy as described below using either $^{16}O_2$ or $^{18}O_2$. The warming of samples of **2a**·O_2 to room temperature, following preparation with $^{18}O_2$, forms a labeled Fe−(^{18}O)−Fe end-product species, as determined by RR spectroscopy {ν_{as}(Fe−^{18}O−Fe) = 803 cm^{-1}}[25] or by FTIR spectroscopy {ν_{as}(Fe−^{18}O−Fe) = 803 cm^{-1}}.

[(^{6}L)Fe(CO)(thf)Fe^{II}−Cl]B(C_6F_5)$_4$ (2a·CO). In the glovebox, a THF solution (12 mL) of [(^{6}L)Fe^{II}···Fe^{II}−Cl]B(C_6F_5)$_4$ (**2a**) (200 mg, ca. 10 mmol) was charged to a 50 mL air-free reaction flask fitted with a rubber septum and subjected to three freeze/pump/thaw cycles, finally leaving it at room temperature under argon. To this static system was added carbon monoxide (10 mL, 1 atm) via syringe with gentle bubbling through the solution. The solution was allowed to stir at room temperature under a CO atomosphere for 2 h and then the solvent was removed under reduced pressure. Recrystallization of the resulting solid from CH_2Cl_2/heptane gave a red microcrystalline product (155 mg, 75%). ^{1}H NMR (THF-d_8, 300 MHz): δ 92 (br), 81 (br), 60 (s), 53−50 (m), 46−42 (m), 39−29 (m), 8.9 (pyrrole-H), −5, −10, −19. UV−Vis (THF, nm): 412, 532. FTIR (film, cm^{-1}) 1969 (ν_{CO}), 1642, 1623, 1605, 1583, 1513, 1463, 1413, 1372, 1333, 1271, 1235, 1201. Anal. Calcd for $C_{93}H_{50}BCl_3F_{26}Fe_2N_8O_3$ (**4**·CH_2Cl_2·C_4H_8O): C, 54.48; H, 2.46; N, 5.47. Found: C, 54.73; H, 2.53; N, 5.16.

[(^{6}L)Fe(NO)Fe(NO)−Cl]B(C_6F_5)$_4$ (2a·$(NO)_2$). In the glovebox, a THF solution (12 mL) of [(^{6}L)Fe^{II}···Fe^{II}−Cl]B(C_6F_5)$_4$ (**2a**) (200 mg, ca. 10 mmol) was charged to a 50 mL air-free reaction flask fitted with a glass stopper. The reaction flask was subjected to three freeze/pump/thaw cycles and finally left frozen in liquid nitrogen under a static vacuum. To this was added nitric oxide (50 mL, 1 atm) and the reaction vessel was subsequently allowed to warm to room temperature as a closed system. The reaction mixture, now a bright orange-red color, was allowed to stir at room tempearture for 4 h. The solvent was then removed under reduced pressure. Recrystallization of the resulting solid from CH_2Cl_2/heptane gave an orange-red powder (140 mg, 70%). ^{1}H NMR (THF-d_8, 300 MHz): δ 159, 142, 135, 130, 126, 116, 101, 93, 87, 76, 64, 61, 60, 55, 51.2, 49, 47, 43, −22, −29, −50. UV−Vis (THF, nm): 412, 545. FTIR (film, cm^{-1}) 1798 (ν_{NO}), 1689 (ν_{NO}), 1642, 1625, 1606, 1583, 1575, 1513, 1462, 1413, 1374, 1344, 1274, 1235, 1204. EPR (THF solution, 198 K): $g \approx 2.0$. Anal. Calcd for $C_{95}H_{58}BCl_3F_{26}Fe_2N_{10}O_3$ (**3**·CH_2Cl_2·C_7H_{16}): C, 54.07; H, 2.77; N, 6.64. Found: C, 53.80; H, 2.36; N, 6.49. MALDI-TOF-MS: *m*/*z* 1247 (M + H$^+$ − BArF$^-$)$^+$.

UV−Visible Spectroscopic Test for Reversible O_2-Binding. In the glovebox, solutions of **2a** were prepared in THF solvent and transferred into a low-temperature quartz cuvette with Schlenk-type air-free sidearm flask. Subsequent cooling of the cuvette assembly to 193 K was followed by direct bubbling of dioxygen into the solution via needle, thereby generating a heme−O_2 adduct. The removal of excess dioxygen was accomplished by application of a vacuum at 193 K. The test for reversible dioxygen binding was carried out by bubbling the solution with a steady stream of dry argon at 193 K for several minutes.

Dioxygen Uptake Determined by Spectrophotometric Titration. Using a published procedure,[44] the dioxygen uptake for room-

(39) Karlin, K. D.; Cruse, R. W.; Gultneh, Y.; Farooq, A.; Hayes, J. C.; Zubieta, J. *J. Am. Chem. Soc.* **1987**, *109*, 2668−2679.
(40) Karlin, K. D.; Haka, M. S.; Cruse, R. W.; Meyer, G. J.; Farooq, A.; Gultneh, Y.; Hayes, J. C.; Zubieta, J. *J. Am. Chem. Soc.* **1988**, *110*, 1196−1207.
(41) Ghiladi, R. A.; Karlin, K. D. *Inorg. Chem.* **2002**, *41*, 2400−2407.
(42) Kopf, M.-A.; Neuhold, Y.-M.; Zuberbuehler, A. D.; Karlin, K. D. *Inorg. Chem.* **1999**, *38*, 3093−3102.
(43) Nanthakumar, A.; Fox, S.; Karlin, K. D. *J. Chem. Soc., Chem. Commun.* **1995**, 499−501.
(44) Ghiladi, R. A.; Kretzer, R. M.; Guzei, I.; Rheingold, A. L.; Neuhold, Y.-M.; Hatwell, K. R.; Zuberbüehler, A. D.; Karlin, K. D. *Inorg. Chem.* **2001**, *40*, 5754−5767.

temperature solutions of $[(^6L)Fe^{II}\cdots Fe^{II}-Cl]^+$ (**2**) was determined using UV−visible spectroscopy. An air-free cuvette assembly was charged with a THF solution of **2**, and then known quantities of dioxygen (from a 1.01% O_2 in Ar gas mixture) were directly bubbled via syringe into the solutions. The reaction mixture was allowed to equilibrate for 12 h before a measurement was made. Measurements indicated that roughly 0.60 or 0.49 (avg ∼0.55) equiv of dioxygen were required for the complete conversion of $[(^6L)Fe^{II}\cdots Fe^{II}-Cl]^+$ (**2**) to $[(^6L)Fe^{III}-O-Fe^{III}-Cl]PF_6$ (**1**). Further injection(s) of dioxygen, in excess of 0.55 equiv of dioxygen, resulted in no further spectroscopic changes.

Dioxygen Evolution during Conversion of 2 to 1. Spectrophotometric measurements, using alkaline pyrogallol solutions, were used to determine dioxygen evolution from low-temperature heme−O_2 adducts according to published procedures.[41,44] Anaerobic THF solutions (12 mL) of $[(^6L)Fe^{II}\cdots Fe^{II}-Cl]^+$ (**2**) (20 mg) were prepared in an air-free flask and fitted with a rubber septum. The solutions were removed from the glovebox and then connected to the vacuum/argon manifold. Solutions of **2** were cooled under an argon atmosphere to 193 K, and then an excess of dioxygen was bubbled through the solution. To remove excess unbound O_2, **2a**·O_2 was subjected to five freeze/pump/thaw cycles with each thaw cycle involving the warming of the solution from liquid nitrogen temperature (77 K) to roughly 193 K. Subsequently, the low-temperature adduct was warmed to room temperature and the dioxygen evolution (0.41, 0.49, 0.52 equiv O_2) was quantified (UV−visible spectroscopy) by pyrogallol trapping.

Nitric Oxide Evolution. The addition of excess axial base to solutions of heme−nitrosyl complexes, resulting in the liberation of NO(g), has been reported.[45] Mixing an excess of 1,5-dicyclohexylimidazole or (dimethylamino)pyridine with THF solutions of $[(^6L)Fe(NO)-Fe(NO)-Cl]B(C_6F_5)_4$ (**2a**·$(NO)_2$) resulted in the evolution of NO(g). Nitric oxide was directly detected in the headspace of the reaction using gas chromatography. Gas chromatography was performed on a Hewlett-Packard 5890 Series II instrument equipped with a thermal conductivity detector (TCD) using a 12 ft Porapak-Q packed column. In a second qualitative method, an air-free cuvette containing a THF solution of $[(F_8)Fe^{II}]$ (**4**) was connected, via rubber tubing, to a flask containing the THF mixture of base/**2a**·$(NO)_2$. The released NO(g) was "trapped" by **4**, resulting in conversion to the complex $[(F_8)Fe(NO)]$ (**4**·NO), as determined by UV−visible spectroscopy.

Resonance Raman (RR) Spectroscopy. RR samples were prepared using a 3−5 mM solution of **2a** in an appropriate solvent. This solution was then transferred to a 5 mm NMR tube and fitted with a rubber septum, placed into a cold bath (193 K) and bubbled with either $^{16}O_2$ or $^{18}O_2$ gas (10 mL) using a Hamilton gastight syringe fitted with an air-free three-way valve. The oxygenated samples were held cold for 10 min, before being frozen in liquid nitrogen and flame-sealed.

RR spectra were obtained using frozen samples thermostated to 90 K with a liquid nitrogen coldfinger. A 413 nm Kr^+ laser (Innova 302, Coherent, Santa Clara, CA) was used for excitation in conjunction with a Kaiser Optical (Ann Arbor, MI) supernotch filter to attenuate Rayleigh scattering. The backscattered light was analyzed with a McPherson (Acton, MA) 2061/207 spectrograph (0.67 m with variable gratings) equipped with a Princeton Instrument (Roper Scientific, Trenton, NJ) liquid-nitrogen cooled (LN-1100PB) charge-coupled device (CCD) detector. Frequencies were calibrated relative to known standards and are within ±1 cm^{-1}. The laser power was kept below 20 mW to minimize sample decomposition and to prevent undesirable photochemical side reactions.

Results and Discussion

Synthesis and Characterization of $[(^6L)Fe^{II}\cdots Fe^{II}-Cl]^+$ (2). The complexes $[(^6L)Fe^{III}-O-Fe^{III}-Cl]B(C_6F_5)_4$ (**1a**) and $[(^6L)Fe^{III}-O-Fe^{III}-Cl]PF_6$ (**1b**), differing only in counteranion identity, were prepared according to literature procedures.[25] A

Scheme 1

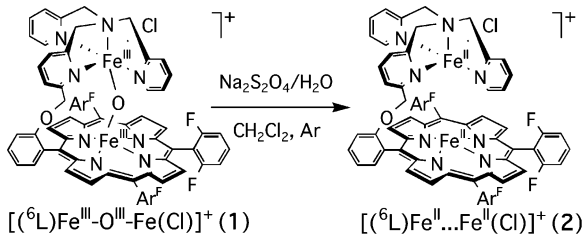

desire to "model" the active site reactivity of the heme/nonheme diiron complexes with relevant substrates such as NO, CO, and O_2 prompted the synthesis of fully reduced analogues of these μ-oxo compounds. Deaerated dichloromethane solutions of the μ-oxo complexes **1a**/**1b** are readily reduced, in a biphasic reaction, using aqueous sodium dithionite to yield either $[(^6L)-Fe^{II}\cdots Fe^{II}-Cl]B(C_6F_5)_4$ (**2a**) or $[(^6L)Fe^{II}\cdots Fe^{II}-Cl]PF_6$ (**2b**), respectively (Scheme 1). The reaction is presumably quantitative; we report isolated yields of ∼80% due to limitations in physically separating the organic compounds (**2a**/**2b**) from the aqueous dithionite solutions.

As expected, $[(^6L)Fe^{II}\cdots Fe^{II}-Cl]B(C_6F_5)_4$ (**2a**) and $[(^6L)Fe^{II}\cdots Fe^{II}-Cl]PF_6$ (**2b**) have identical UV−visible signatures in THF solvent, with very intense Soret transitions at $\lambda_{max} = 424$ nm ($\epsilon = 205000\ M^{-1}\ cm^{-1}$). Of lesser intensity are the Q-bands at $\lambda_{max} = 544$ nm ($\epsilon = 9900\ M^{-1}\ cm^{-1}$). These features are consistent with those of known ferrous heme compounds in coordinating solvents.[41,44] It should be noted that the UV−visible features are dominated by porphyrin-based $\pi \rightarrow \pi^*$ transitions ($\epsilon \approx 10000-200000\ M^{-1}\ cm^{-1}$) which precludes the observation of the expected much weaker (TMPA)Fe^{II} absorption ($\lambda_{max} \approx 400$ nm, $\epsilon \approx 3000\ M^{-1}\ cm^{-1}$).[46]

Examination of the ^1H NMR spectrum of **2a** in THF-d_8 reveals an array of paramagnetically shifted proton signals, Figure 2, ranging downfield from 91 ppm to upfield at −19

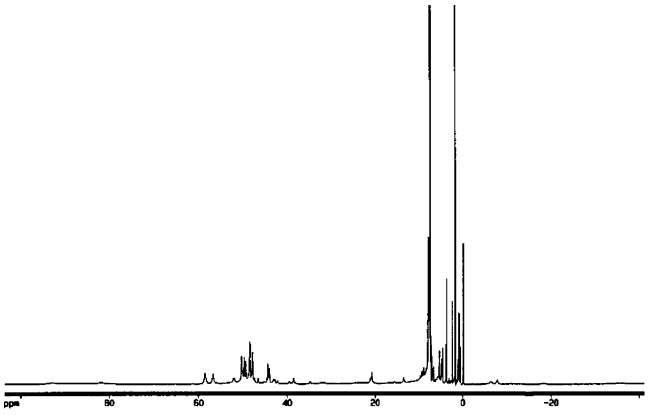

Figure 2. Proton NMR spectrum of $[(^6L)Fe^{II}\cdots Fe^{II}-Cl]B(C_6F_5)_4$ (**2a**), recorded at 298 K in THF-d_8.

ppm. The spectrum represents of juxtaposition of proton signals arising from the influence of the two independent high-spin Fe^{II} ion centers, with paramagnetic resonances observed for (presumably) pyrrole, pyridyl (TMPA), and methylene (TMPA) protons. The spectrum is further complicated by the inherent lack of symmetry (as compared with the ^6L μ-oxo compounds),[25] as the tethered-TMPA portion of the system is no longer

(45) Bohle, D. S.; Hung, C.-H. *J. Am. Chem. Soc.* **1995**, *117*, 9584−9585.

(46) Kojima, T.; Leising, R. A.; Yan, S.; Que, L., Jr. *J. Am. Chem. Soc.* **1993**, *115*, 11328−35.

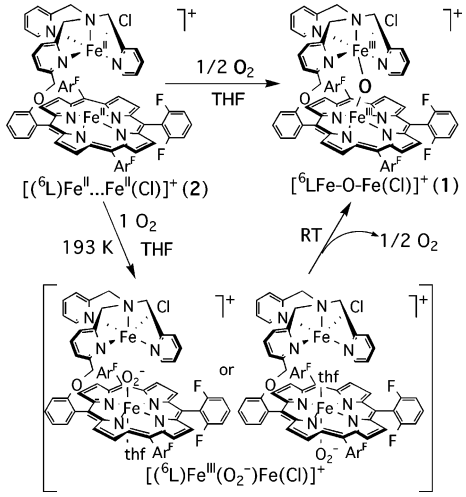

Figure 3. Reaction of the reduced complex $[(^6L)Fe^{II}\cdots Fe^{II}-Cl]^+$ (**2**) with dioxygen, to form a μ-oxo complex $[(^6L)Fe^{III}-O-Fe^{III}-Cl]$ (**1**), via a low-spin heme$-O_2$ ($Fe^{III}-O_2^-$) intermediate. The stoichiometries of reactions and incorporation of O-label into **1** have been confirmed, see text.

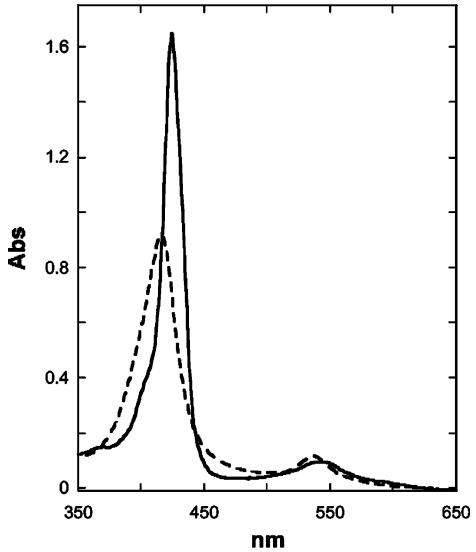

Figure 4. UV−visible spectrum (THF, 193 K) of $[(^6L)Fe^{II}\cdots Fe^{II}-Cl]B(C_6F_5)_4$ (**2a**) (solid trace; λ_{max} 424, 544 nm) and the spectrum of the resulting dioxygen adduct $[(^6L)Fe^{III}(O_2^-)\cdots Fe^{II}-Cl]B(C_6F_5)_4$ (**2a**·O_2) (dashed trace; λ_{max} 414, 536 nm).

"anchored" directly to the porphyrin iron and we expect considerable room-temperature fluxionality of the TMPA-tether (relative to the plane of the porphyrin). Reasonable assignments include the following: (1) Pyrrole proton resonances found as a set of multiplets between 47 and 50 ppm and a singlet near 21 ppm, consistent with other synthetic five-coordinate high-spin hemes in THF-d_8.[18,24,41,44] (2) Pyridyl-H and methylene $-CH_2-$ (TMPA) proton resonances observed at 91, 82, 59, 57, 46−44, 43−35, −6.1, −7.5, and −19 ppm. The assignments of the TMPA-Fe proton resonances are consistent with the work of Que and co-workers,[47] who have noted that the inclusion of a methyl substituent in the 6-pyridyl position in $(TMPA)Fe^{II}$ complexes (i.e., as occurs here for one of the pyridyl donor groups in the ligand ^6L) favors iron ions with larger ionic radii (e.g., high-spin Fe(II)). Such $S = 2$ complexes have paramagnetically shifted proton resonances, typically between −24 and 95 ppm.[47]

Reactivity of Dioxygen with $[(^6L)Fe^{II}\cdots Fe^{II}-Cl]^+$ (2). Addition of an excess of dioxygen to room-temperature solutions of $[(^6L)Fe^{II}\cdots Fe^{II}-(Cl)]B(C_6F_5)_4$ (**2a**) in THF results in the clean formation of $[(^6L)Fe^{III}-O-Fe^{III}-Cl]B(C_6F_5)_4$ (**1a**) (Figure 3). Room-temperature spectrophotometric titrations (see Experimental Section) of **2a** with dioxygen in THF reveal that 0.55 equiv of dioxygen are required to form 1 equiv of $[(^6L)Fe^{III}-O-Fe^{III}-Cl]B(C_6F_5)_4$ (**1a**). However, an intermediate is observed by direct bubbling of O_2 (∼30 s) into a *cold* (193 K) THF solution of $[(^6L)Fe^{II}\cdots Fe^{II}-Cl]B(C_6F_5)_4$ (**2a**) {$\lambda_{max} = 424$ (Soret) and 544 nm}; this is formulated as a heme−superoxo complex $[(^6L)Fe^{III}(O_2^-)\cdots Fe^{II}-Cl)]B(C_6F_5)_4$ (**2a**·O_2), having UV−visible features at 318, 414 (Soret), and 536 nm (Figures 3 and 4). This finding is similar to that observed for related complexes $[(^6L)Fe^{II}]$ (**3**) and $[(F_8)Fe^{II}]$ (**4**) (Chart 1), which also form heme−superoxo adducts in THF solvent, $[(^6L)Fe(O_2^-)]$ (**3**·O_2)[41] and $[(F_8)Fe(O_2^-)]$ (**4**·O_2),[20,44] respectively. While O_2-binding to **3** and **4** is reversible, the formation of $[(^6L)Fe^{III}(O_2^-)\cdots Fe^{II}-Cl)]B(C_6F_5)_4$ (**2a**·O_2), derived from the heme/non-heme diiron(II) complex **2a**, is not. Direct bubbling of argon or application of a vacuum *does not* result in the release of dioxgyen. These results suggest that either the non-heme iron stabilizes the heme−dioxygen interaction in $[(^6L)Fe^{III}(O_2^-)\cdots Fe^{II}-Cl]B(C_6F_5)_4$ (**2a**·O_2) or an alternative decomposition pathway (i.e., other than simple loss of O_2) is readily available. Warming of **2a**·O_2 to room temperature cleanly produces the μ-oxo complex $[(^6L)Fe^{III}-O-Fe^{III}-Cl]B(C_6F_5)_4$ (**1a**) (Figure 3) with the evolution of ∼0.5 equiv of dioxygen (see Experimental Section), consistent with the stoichiometric relationships between **2**, **1**, and **3**, those indicated in Figure 3.

Resonance Raman (RR) Spectroscopy. Low-temperature (90 K) laser excitation (413 nm) into the Soret band of $[(^6L)Fe^{II}\cdots Fe^{II}-Cl]B(C_6F_5)_4$ (**2a**) in THF yields a RR spectrum dominated by porphyrin skeletal modes.[48] The ν_4 and ν_2 modes are observed at 1345 and 1537 cm^{-1}, respectively, indicating **2a** is best formulated as a high-spin ferrous complex (see Supporting Information, Figure S1). Indeed, for typical five-coordinate high-spin $[(P)Fe^{II}]$, the oxidation-state marker ν_4 is observed at 1342 cm^{-1} and the spin-state marker ν_2 is at 1537 cm^{-1}.[48,49] These results and assignments are consistent with the ^1H NMR pyrrole proton resonance assignment (vide supra) suggesting an $S = 2$, high-spin heme complex with an axial THF ligand for **2a**. In contrast, porphyrin skeletal modes in the high-frequency region for the dioxygen complex $[(^6L)Fe^{III}(O_2^-)\cdots Fe^{II}-Cl]B(C_6F_5)_4$ (**2a**·O_2) indicate the presence of a low-spin ferric heme species with marker bands (ν_4 and ν_2) at 1370 cm^{-1} and 1572 cm^{-1}, respectively, by comparison with other known low-spin $[(TPP)Fe^{III}]$ compounds (ν = 1370, 1568 cm^{-1}).[49] Presumably, the formally ferric-heme in **2a**·O_2 is coordinated by axial superoxo (O_2^-) and THF ligands (Figure 3), giving an overall six-coordinate low-spin complex, as is well known.[41,44] The hexa-coordinated nature of the superoxo complex is confirmed by the frequency displayed by the $\nu(Fe-O_2)$ described below.

An earlier, less detailed study[24] showed that an analogue complex of $[(^6L)Fe^{II}\cdots Fe^{II}-Cl]^+$ (**2**), $[(^5L)Fe^{II}\cdots Fe^{II}-Cl]^+$, was

(47) Zang, Y.; Kim, J.; Dong, Y.; Wilkinson, E. C.; Appelman, E. H.; Que, L., Jr. *J. Am. Chem. Soc.* **1997**, *119*, 4197−4205.

(48) Nakamoto, K. *Infrared and Raman Spectra of Inorganic and Coordination Compounds*; Wiley-Interscience: New York, 1997.

(49) Burke, J. M.; Kincaid, J. R.; Peters, S.; Gagne, R. R.; Collman, J. P.; Spiro, T. G. *J. Am. Chem. Soc.* **1978**, *100*, 6083−6088.

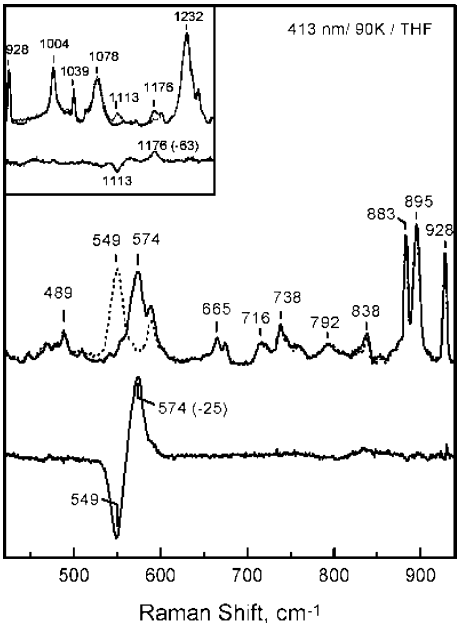

Figure 5. RR spectra of $[(^6L)Fe^{III}(O_2^-)\cdots Fe^{II}-Cl]B(C_6F_5)_4$ (**2a**·O_2^-) formed by oxygenation with either $^{16}O_2$ (solid trace) or $^{18}O_2$ (dashed trace). The difference spectrum ($^{16}O - {}^{18}O$) is shown as the bottom trace. The inset shows the high-frequency region using both $^{16}O_2$ (solid trace) or $^{18}O_2$ (dashed trace), with the bottom trace showing the difference spectrum ($^{16}O - {}^{18}O$). The spectra were recorded at 90 K using 413 nm excitation.

observed to form a low-temperature stable dioxygen adduct, but whether dioxygen was bound as a peroxo or a superoxo ligand was not ascertained. Here, however, examination of the mid-frequency RR regions for $[(^6L)Fe^{III}(O_2^-)\cdots Fe^{II}-Cl]B(C_6F_5)_4$ (**2a**·O_2) confirms that dioxygen is bound as a superoxo (O_2^-) entity (Figure 5). RR spectra of **2a**·O_2, prepared with $^{16}O_2$ gas, reveals a ν(O−O) at 1176 cm^{-1}, that downshifts by 63 cm^{-1} to 1113 cm^{-1} with $^{18}O_2$ gas. In the low-frequency region, the ν(Fe−O) is detected at 574 cm^{-1} and shifts by −25 cm^{-1} with $^{18}O_2$ gas. These frequencies unambiguously identify **2a**·O_2 as a hexa-coordinated iron(III)-superoxo end-on complex.[48,50,51] Warming the $^{16}O_2$ and $^{18}O_2$ superoxo adducts **2a**·O_2 to room temperature re-forms $[(^6L)Fe^{III}-O-Fe^{III}-Cl]B(C_6F_5)_4$ (**1a**), with concomitant incorporation of the labeled oxygen species into the Fe−O−Fe bridge, based upon observed ν_{as}(Fe−^{16}O−Fe) {844 cm^{-1}} and ν_{as}(Fe−^{18}O−Fe) {803 cm^{-1}} stretching frequencies, by either RR or FTIR spectroscopies.[25] Thus, the bridging oxo ligand is derived from dioxygen (Figure 3).

Direct bubbling of dioxygen into low-temperature (198 K) THF solutions of the "empty tether" complex $[(^6L)Fe^{II}]$ (**3**) (Chart 1) also results in the formation of a low-temperature stable superoxo intermediate (Figure 6), $[(^6L)Fe^{III}(O_2^-)]$ (**3**·O_2), which has been previously characterized by UV−visible and NMR spectroscopies.[41] This dioxygen complex is a low-spin six-coordinate species with an axial THF ligand. Here, RR spectroscopic insights are provided (Supporting Information, Figure S2), obtained using either $^{16}O_2$ or $^{18}O_2$, which confirm the presence of a superoxo complex with a ν(O−O) = 1176 cm^{-1} ($\Delta(^{18}O_2)$ −64 cm^{-1}) and a ν(Fe−O) = 572 cm^{-1} ($\Delta(^{18}O_2)$ −24 cm^{-1}). The close similarity in vibrational

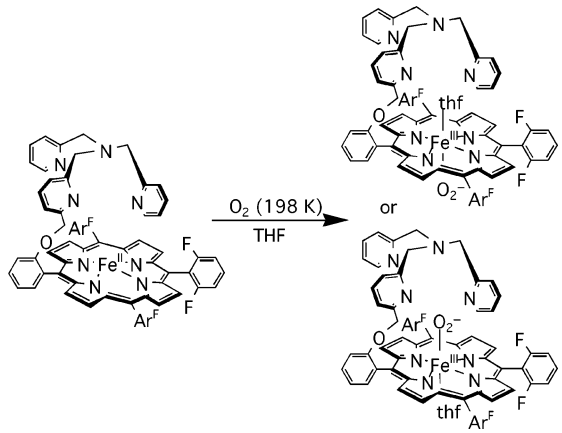

Figure 6. Empty tether complex $[(^6L)Fe^{II}]$ (**3**) reacts with dioxygen to give a low-temperature heme−superoxo adduct **3**·O_2. Dioxygen may perhaps bind to either the top or the bottom face of the tethered heme.

Scheme 2

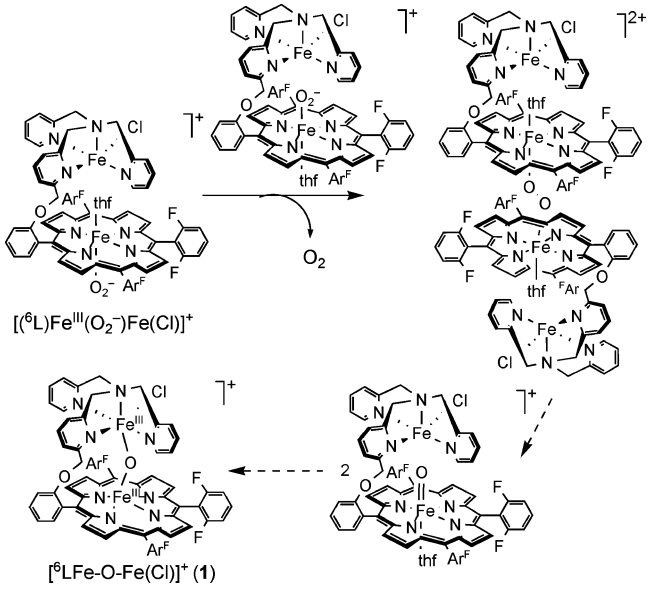

signatures between the complexes $[(^6L)Fe^{III}(O_2^-)\cdots Fe^{II}-Cl]B(C_6F_5)_4$ (**2a**·O_2) and $[(^6L)Fe^{III}(O_2^-)]$ (**3**·O_2) indicates that the non-heme iron does not influence the O−O or Fe−O stretching vibrations when dioxygen binds to the heme iron in **2a**·O_2. THF solutions (193 K) of $[(F_8)Fe^{II}(O_2^-)]$ (**4**·O_2), formed by reaction of $[(F_8)Fe^{II}]$ (**4**) + O_2 (Chart 1), have similar RR vibrational properties.[52]

Proposed Mechanism for μ-Oxo Formation. Several TMPA−Fe complexes with methyl substituents in the 6-pyridyl positions, in the absence of ancillary O-donor ligands, generally have high redox potentials that favor Fe^{II} over the Fe^{III} oxidation state.[47] Thus, given the stoichiometry of reactions observed (Figure 3) and the clear characteristics of $[(^6L)Fe^{III}(O_2^-)\cdots Fe^{II}-Cl]B(C_6F_5)_4$ (**2a**·O_2), we infer that the non-heme iron(II) in **2a** does *not* bind O_2 and that the heme−superoxo moiety in **2a**·O_2 is the sole dioxygen intermediate observed at 193 K.

Scheme 2 provides a proposed series of reactions which may account for a dioxygen (formally, superoxide) disproportion-

(50) Proniewicz, L. M.; Paeng, I. R.; Nakamoto, K. *J. Am. Chem. Soc.* **1991**, *113*, 3294−3303.
(51) Vogel, K. M.; Kozlowski, P. M.; Zgierski, M. Z.; Spiro, T. G. *J. Am. Chem. Soc.* **1999**, *121*, 9915−9921.
(52) Kim, E.; Helton, M. E.; Wasser, I. M.; Karlin, K. D.; Lu, S.; Huang, H.-W.; Moënne-Loccoz, P.; Incarvito, C. D.; Rheingold, A. L.; Honecker, M.; Kaderli, S.; Zuberbuhler, A. D. *Proc. Natl. Acad. Sci. U.S.A.* **2003**, *100*, 3623−8.

ation, starting from **2a**·O_2 and forming the μ-oxo complex [(^{6}L)-Fe^{III}−O−Fe^{III}−Cl]B(C_6F_5)$_4$ (**1a**). The disproportionation reaction stoichiometry is (eq 2)

$$\underset{(\mathbf{2a}\cdot O_2)}{2Fe^{III}-(O_2^{-})\cdots Fe^{II}} \rightarrow O_2 + \underset{\mathbf{1a}}{2Fe^{III}-(O_2^{-})-Fe^{III}} \quad (2)$$

Superoxo compound **2a**·O_2 combines with a second equivalent of **2a**·O_2, forming an intermolecular heme−peroxo−heme complex, while releasing an equivalent of dioxygen. Subsequent thermally induced (i.e. warming) cleavage of the O−O bond would result in a short-lived mixed-valent heme ferryl/non-heme ferrous complex, which could then combine with the non-heme iron(II) in an intramolecular fashion to give the diferric μ-oxo product [(^{6}L)Fe^{III}−O−Fe^{III}−Cl]B(C_6F_5)$_4$ (**1a**). Similar mechanisms, involving μ-peroxo diferric heme or non-heme diiron compounds that thermally decompose to yield μ-oxo diferric systems, are known.[53−58] Attempts to identify a peroxo intermediate here, e.g., [heme Fe−O−O−Fe heme] or [heme Fe−O−O−Fe non-heme] species, have been unsuccessful.

Synthesis of Monocarbonyl Compound [(^{6}L)Fe^{II}(CO)(thf)-Fe^{II}−Cl]B(C_6F_5)$_4$ (2a·CO). Solutions of [(^{6}L)$Fe^{II}\cdots Fe^{II}$−Cl]B-(C_6F_5)$_4$ (**2a**) in THF were bubbled with an excess of carbon monoxide at room temperature, turning from red to peach in color, to give a compound formulated as [(^{6}L)Fe^{II}(CO)(thf)-Fe^{II}−Cl]B(C_6F_5)$_4$ (**2a**·CO) (Chart 1). The complex could be isolated as a solid. In THF solutions, **2a**·CO exhibits UV−visible features at 412 (Soret) and 532 nm. Similar spectral changes have been observed upon carbonylation of the "empty tether" complex [(^{6}L)Fe^{II}] (**3**) {λ_{max} = 424, 543 nm} to form the corresponding carbonyl complex [(^{6}L)Fe^{II}(CO)] (**3**·CO) {λ_{max} = 413 (Soret), 532 nm}.[59] Similarly, the parent complex [(F_8)Fe(CO)] has electronic transitions that support the above formulation of **2a**·CO.[60] Other synthetic heme−CO and natural heme−CO complexes show UV−vis features of a similar nature.[61,62]

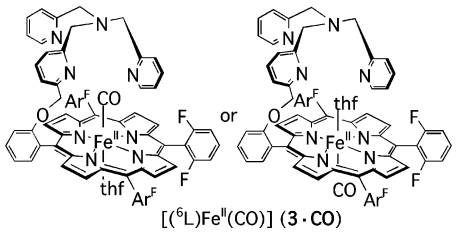

An IR spectrum of **2a**·CO, obtained by evaporating a concentrated THF solution of **2a**·CO onto an IR window, showed a prominent new band (compared to **2a**) at ν(CO) = 1969 cm^{-1} (Supporting Information, Figure S3), consistent with the presence of a mononuclear heme carbonyl species and indicating that the CO ligand is not bridging the two iron sites.[48] Typical non-heme iron−carbonyl complexes are limited to binary carbonyl and cyclopentadienyl ligand systems;[63] the non-heme iron in **2a** appears to have little affinity for CO. A comparison of the heme−CO stretching vibrations of the complex **2a**·CO {$\nu(CO)_{Fe}$ 1969 cm^{-1}} to the CO vibration of the empty-tether complex [(^{6}L)Fe^{II}(CO)] (**3**·CO) in THF {$\nu(CO)_{Fe}$ = 1976 cm^{-1}} or [(F_8)Fe(CO)] in THF {$\nu(CO)_{Fe}$ = 1979 cm^{-1}} suggests that **2a**·CO posesses a six-coordinate, heme−CO moiety, with THF as a likely axial ligand.[59,60] Axial ligation by THF in [(F_8)(thf)Fe(CO)] has been established by an X-ray crystal structure of this six-coordinate low-spin heme compound.[60]

A ^{1}H NMR spectrum for [(^{6}L)Fe^{II}(CO)(thf)Fe^{II}−Cl]B(C_6F_5)$_4$ (**4**) (Supporting Information, Figure S4) recorded in THF-d_8 reveals a "simplification" of the paramagnetic region relative to the diferrous complex [(^{6}L)$Fe^{II}\cdots Fe^{II}$−Cl]B(C_6F_5)$_4$ (**2a**). The most prominent change is the loss of signals between 40 and 60 ppm and a appearance of new, broad resonance near 8.9 ppm, corresponding to the pyrrole protons. Similar upfield shifts in the ^{1}H NMR pyrrole resonances have been observed upon addition of CO to the complex (^{6}L)Fe^{II} in THF-d_8 {50−60 ppm → 9 ppm}.[59] Such a change in pyrrole-proton resonances is indicative of a spin-state change: from a five-coordinate high-spin, ferrous heme to a six-coordinate, low-spin diamagnetic ferrous heme−carbonyl. As already described, **2a**·CO incorporates an axial THF ligand derived from the bulk solvent. However, we are unable to observe the ^{1}H NMR signals derived from the coordinated THF ligand, due to the expected rapid exchange with the bulk NMR solvent. The non-heme iron site, which is not found to bind CO, remains a high-spin ferrous ion, with paramagnetically shifted signals similar to those observed for [(^{6}L)$Fe^{II}\cdots Fe^{II}$−Cl]B(C_6F_5)$_4$ (**2a**). Thus, this tethered TMPA Fe_B site is not affected by coordination of carbon monoxide at the adjacent heme.

Synthesis of Dinitrosyl Complex [(^{6}L)Fe(NO)Fe(NO)−Cl]B(C_6F_5)$_4$ (2a·$(NO)_2$). Distillation of an excess of NO(g) onto a frozen THF solution of [(^{6}L)$Fe^{II}\cdots Fe^{II}$−Cl]B(C_6F_5)$_4$ (**2a**) and subsequent warming to room temperature resulted in a color change from red to red-orange. The product complex [(^{6}L)Fe-(NO)Fe(NO)−Cl]B(C_6F_5)$_4$ (**2a**·$(NO)_2$) was isolated after recrystallization from CH_2Cl_2/heptane. Tetrahydrofuran solutions of **2a**·$(NO)_2$ have a UV−visible spectrum dominated by porphyrin-based electronic transitions at 412 (Soret) and 545 nm. Similarly, toluene solutions of [(^{6}L)Fe(NO)Fe(NO)−Cl]B-(C_6F_5)$_4$ (**2a**·$(NO)_2$) have transitions at 408 (Soret) and 542 nm. Farmer and co-workers[64] have reported an electronic absorption spectrum for [(TPP)Fe−NO] in toluene as λ_{max} 407 (Soret), 537 nm, while Ford and co-workers[65] described a similar spectrum for the same compound in toluene (λ_{max} 406 (Soret), 539 nm). These observations indicate that the heme portion of [(^{6}L)Fe-(NO)Fe(NO)−Cl]B(C_6F_5)$_4$ (**2a**·$(NO)_2$) consists of a five coordinate heme−nitrosyl, similar to (TPP)Fe−NO and related complexes. The intense heme-based electronic transitions

(53) Balch, A. L. *Inorg. Chim. Acta* **1992**, *198−200*, 297−307.
(54) Balch, A. L.; Chan, Y.-W.; Cheng, R.-J.; La Mar, G. N.; Latos-Grazynski, L.; Renner, M. W. *J. Am. Chem. Soc.* **1984**, *106*, 7779−7785.
(55) Chiou, Y.-M.; Que, J. L. *J. Am. Chem. Soc.* **1995**, *117*, 3999−4013.
(56) Lee, D.; Pierce, B.; Krebs, C.; Hendrich, M. P.; Huynh, B. H.; Lippard, S. J. *J. Am. Chem. Soc.* **2002**, *124*, 3993−4007.
(57) Feig, A. L.; Lippard, S. J. *Chem. Rev.* **1994**, *94*, 759−805.
(58) DuBois, J.; Mizoguchi, T. J.; Lippard, S. J. *Coord. Chem. Rev.* **2000**, *200−202*, 443−485.
(59) Kretzer, R. M.; Ghiladi, R. A.; Lebeau, E. L.; Liang, H.-C.; Karlin, K. D. *Inorg. Chem.* **2003**, *42*, 3016−3025.
(60) Thompson, D. W.; Kretzer, R. M.; Lebeau, E. L.; Scaltrito, D. V.; Ghiladi, R. A.; Lam, K.-C.; Rheingold, A. L.; Karlin, K. D.; Meyer, G. J. *Inorg. Chem.* **2003**, *42*, 5211−5218.
(61) Tsuchida, E.; Komatasu, T.; Arai, K.; Hishide, H. *J. Chem. Soc., Dalton Trans.* **1993**, 2465−2469.
(62) Collman, J. P.; Brauman, J. I.; Doxsee, K. M.; Halbert, T. R.; Bunnenberg, E.; Linder, R. E.; La Mar, G. N.; Del Gaudio, J.; Lang, G.; Spartalian, K. *J. Am. Chem. Soc.* **1980**, *102*, 4182−4192.
(63) Cotton, F. A.; Wilkinson, G.; Bochmann, M.; Murillo, C. *Advanced Inorganic Chemistry, 6th ed.;* John Wiley & Sons: New York, 1998.
(64) Lin, R.; Farmer, P. J. *J. Am. Chem. Soc.* **2001**, *123*, 1143−1150.
(65) Lorkovic, I.; Ford, P. C. *Inorg. Chem.* **2000**, *39*, 632−633.

preclude the observation of absorption signals which could be assigned to the (TMPA)Fe(NO)(Cl) portion of the system, which are expected near λ_{max} 350 nm, but with small extinction coeffecient ($\epsilon \approx 1000\ M^{-1}\ cm^{-1}$).[66]

Freshly prepared THF solutions of [(^{6}L)Fe(NO)Fe(NO)−Cl]B(C_6F_5)$_4$ (**2a·**(NO)$_2$) were used to prepare air-free samples for MALDI mass spectrometry (see Experimental Section). The spectrum (Supporting Information, Figure S5) is dominated by a parent ion peak at *m*/*z* 1247 amu corresponding to [(^{6}L)Fe(NO)Fe(NO)−Cl]$^+$ or a (M + H$^+$ − B(C_6F_5)$_4^-$)$^+$ cation. A fragment ion peak corresponding to the loss of a single nitrosyl ligand is not observed; rather, both nitrosyl ligands are lost to give rise to a fragment with *m*/*z* 1186 amu which is tentatively assigned as a (M − 2NO − B(C_6F_5)$_4^-$)$^+$ cation. The appearance of the fragment ion peak at *m*/*z* 1167 amu suggests the presence of an ion related to [(^{6}L)Fe^{III}−O−Fe^{III}−Cl]B(C_6F_5)$_4$ (**1a**), specifically an (M + H$^+$ − Cl − B(C_6F_5)$_4^-$)$^+$ cation. The observation of the μ-oxo species suggests that either; (a) the sample is partially oxidized during transfer from the reaction tube to the mass spectrometer; or (b) (we speculate) laser excitation is of sufficient energy to cause the photorelease and coupling of the nitrosyl ligands, resulting in the formation of [(^{6}L)Fe^{III}−O−Fe^{III}−Cl]$^+$ (**1**) within the mass spectrometer.

The proton NMR spectrum for [(^{6}L)Fe(NO)Fe(NO)−Cl]B(C_6F_5)$_4$ (**2a·**(NO)$_2$) (Supporting Information, Figure S6) reveals an array of paramagnetically shifted signals from 159 to −50 ppm. Such a wide range of signals might be expected due to the presence of two paramagnetic Fe-nitrosyl species. Similar up- and downfield shifted paramagnetic NMR signals have been reported by Que and co-workers for [(TMPA)Fe(NO)] complexes.[66] Likely proton assignments, by analogy to the work of Que and co-workers, include the following: (1) methylene −CH_2− resonances at 159, 142, and 126 ppm; (2) α-H pyridyl proton resonances at 101, 116, and 93 ppm; (3) β,β'-H pyridyl proton resonances at 87, 76, 64, 61, 60, and 55 ppm. The remaining proton signals (−22, −29, −50 ppm), that are found upfield from TMS, presumably arise from the γ-H pyridyl protons. Iron nitrosyl complexes of the formulation {FeNO}^{7} (see also discussion below) are paramagnetic species with a spin delocalized electron over both the Fe ion and the NO ligand.[67,68] Therefore, it should also be noted that the pyrrole and other proton resonance from heme−nitrosyl species are often broad and unobserved;[69] hence, no definitive assignment for the pyrrole proton resonance of [(^{6}L)Fe(NO)Fe(NO)−Cl]B(C_6F_5)$_4$ (**2a·**(NO)$_2$) is given here.

Complex (**2a·**(NO)$_2$) exhibits a room-temperature EPR spectrum with an intense resonance at $g \approx 2.0$ (see Experimental Section), which would be characteristic of heme−NO species.[45,68] An EPR signal derived from the non-heme iron−nitrosyl site, expected at $g \approx 4$,[66,70] was not observed.

[(^{6}L)Fe(NO)Fe(NO)−Cl]B(C_6F_5)$_4$ (2a·(NO)$_2$): Infrared Spectroscopy. The confirmation of nitrosyl ligand coordination at both the heme and the non-heme iron sites required infrared spectroscopy. FTIR spectra obtained from solid film samples of [(^{6}L)Fe(NO)Fe(NO)−Cl]B(C_6F_5)$_4$ (**2a·**(NO)$_2$) revealed two new stretching vibrations, relative to the reduced [(^{6}L)Fe^{II}···Fe^{II}−Cl]B(C_6F_5)$_4$ (**2a**), at 1798 and 1689 cm^{-1} (Figure 7). The ν_{NO} signal intensities are not equivalent, suggesting unequal populations of the heme and non-heme iron−nitrosyl sites. This is likely due to some exposure of the solid FTIR samples to the ambient atmosphere during the spectral measurement, likely leading to partial product decomposition. A complete bleach of the non-heme iron−nitrosyl ν_{NO} was observed within an hour while the heme−nitrosyl ν_{NO} decayed at a somewhat slower rate. These bands were shifted to 1756 and 1652 cm^{-1} when ^{15}NO(g) was used in sample preparation. These bands are assigned to heme−NO and non-heme Fe−NO on the basis of values reported in the literature for mononuclear heme−NO and mononuclear non-heme Fe−NO complexes (Table 1). In addition to this criteria, it is known[69] that dinitrosyl heme complexes (e.g., [(P)Fe(NO)$_2$]) do not form at room temperature and complexes of the type [(TMPA)Fe(NO)$_2$] would require a second vacant coordination site at the non-heme iron.[70] These alternative structural formulations can thus be discarded.

Solid film samples of [(^{6}L)Fe^{II}···Fe^{II}−Cl]B(C_6F_5)$_4$ (**2a**) were also prepared on the RIR ATR probe tip (see Experimental Section). Subsequent evacuation and exposure to NO(g) demonstrated the similar in situ formation of [(^{6}L)Fe(NO)Fe(NO)−Cl]B(C_6F_5)$_4$ (**2a·**(NO)$_2$), based upon the new peaks observed at 1798 and 1687 cm^{-1} (Supporting Information, Figure S7).

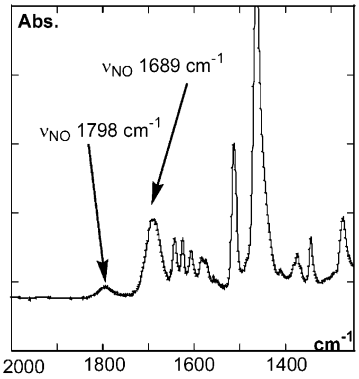

Figure 7. FTIR spectrum for [(^{6}L)Fe(NO)Fe(NO)−Cl]B(C_6F_5)$_4$ (**2a·**(NO)$_2$). Non-heme Fe−NO; ν_{NO} = 1798 cm^{-1}. Heme nitrosyl; ν_{NO} = 1689 cm^{-1}.

Table 1. Iron−Nitrosyl Compounds for Comparison to [(^{6}L)Fe(NO)Fe(NO)−Cl]$^+$ (**2·**(NO)$_2$)

complex	ν_{NO}, cm^{-1}	sample type	ref
[(^{6}L)Fe(NO)$_2$Fe(Cl)]$^+$ (**2·**(NO)$_2$)	1798[a]	film	this work
[(^{6}L)Fe(NO)$_2$Fe(Cl)]$^+$ (**2·**(NO)$_2$)	1689[b]	film	this work
[(TMPA)Fe(NO)(BF)]$^+$	1794	KBr pellet	66
[(TMPzA)Fe(NO)(Cl)]$^+$	1796	KBr pellet	66
[(Me$_3$TACN)Fe(NO)(N$_3$)$_2$]	1690	KBr pellet	71
[(F_{20}-TPP)Fe(NO)]	1705	KBr pellet	45
[(F_8-TPP)Fe(NO)]	1656	film	this work
[(F_8-TPP)Fe(NO)]	1687	KBr pellet	45
[(TMP)Fe(NO)]	1676	KBr pellet	45
[(TPP)Fe(NO)]	1677[c]	film	64
[(TPP)Fe(NO)]	1697[d]	film	64

[a] Tentatively assigned as a non-heme Fe−NO (see text for further discussion). [b] Tentatively assigned as a heme Fe−NO (see text for further discussion). [c] Deposited from wet solvent. [d] After drying film under stream of N_2 for 1 h. Abbreviations used: TPP = tetraphenylporphyrinate dianion; TMP = tetramesitylporphyrinate dianion; F_{20}-TPP = aryl perfluorinated tetraphenylporphyrinate dianion; Me$_3$TACN = *N*,*N*′,*N*″-trimethyl-1,4,7-triazacyclononane; TMPzA = tris((3,5-dimethyl-1-pyrazolyl)methyl)amine.

(66) Chiou, Y.-M.; Que, J, L. *Inorg. Chem.* **1995**, *34*, 3270−3278.
(67) Walker, F. A. In *Porphyrin Handbook*; Kadish, K. M., Smith, K. M., Guilard, R., Eds.; Academic Press: New York, 2000; Vol. 5, pp 81−183.
(68) Cheng, L.; Richter-Addo, G. B. In *The Porphyrin Handbook*; Kadish, K. M., Smith, K. M., Guilard, R., Eds.; Academic Press: New York, 2000; Chapter 33.
(69) (a) Lorkovic, I.; Ford, P. C. *J. Am. Chem. Soc.* **2000**, *122*, 6516−6517. (b) Wayland, B. B.; Olson, L. W. *J. Am. Chem. Soc.* **1974**, *96*, 8037−8041.
(70) Jo, D.-H.; Chiou, Y.-M.; Que, J. L. *Inorg. Chem.* **2001**, *40*, 3181−3190.

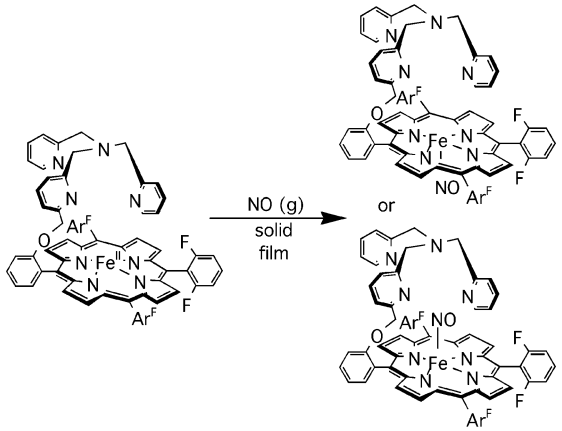

Figure 8. Reaction of empty tether complex [(^{6}L)Fe^{II}] (**3**) with NO(g) to form the five-coordinate heme nitrosyl [(^{6}L)Fe^{II}(NO)] (**3**·NO). The NO ligand is surmised to be either on the top or bottom face of the heme.

A rough plot of absorbance against time (Supporting Information, Figure S7) reveals that the $[FeNO]_2$ species is formed at the heme and non-heme Fe_B sites at similar rates with apparent rapid saturation behavior. Additional clarity comes from the addition of purified NO(g) to THF solutions of the "empty tether" complex [(^{6}L)Fe^{II}] (**3**) (Figure 8), which resulted in the clean formation of a heme nitrosyl (ν_{NO} = 1683 cm^{-1}; Supporting Information, Figure S8). This finding suggests that the heme nitrosyl portion of [(^{6}L)Fe(NO)Fe(NO)−Cl]B(C_6F_5)$_4$ (**2a**·$(NO)_2$) is unperturbed by the presence of a non-heme iron NO ligand.

According to Enemark−Feltham notation, the electrons in an {MNO}^{n} system are counted as if this fragment were completely isolated and *n* corresponds to the number of metal d-electrons plus the electron in the π^* orbitals of the NO.[72] Thus, typical (P)Fe^{II}−NO compounds are formally considered {MNO}^{7} species. By contrast, a ferric nitrosyl (P)Fe^{III}−NO complex could formally be considered an {MNO}^{6} species. For [(^{6}L)Fe(NO)-Fe(NO)−Cl]B(C_6F_5)$_4$ (**2a**·$(NO)_2$), there are two separate {MNO}^{n} fragments. The heme−nitrosyl (ν_{NO} 1689 cm^{-1}) which is spectroscopically similar to (TPP)Fe−NO, therefore, suggests an {FeNO}^{7} formulation.[73,74] Similarly, by comparison to the work of Que and co-workers in their synthesis of (TMPA)Fe−NO complexes, the non-heme nitrosyl (ν_{NO} 1795 cm^{-1}) in **2a**·$(NO)_2$ is also an {FeNO}^{7} system.[31,66] Thus, overall the complex [(^{6}L)Fe(NO)Fe(NO)−Cl]B(C_6F_5)$_4$ (**2a**·$(NO)_2$) is best described, in terms of Enemark−Feltham notation, as [{FeNO}^{7}]$_2$.

Special caution must be taken to ensure the use of pure NO-(g) in the preparation of [(^{6}L)Fe(NO)Fe(NO)−Cl]B(C_6F_5)$_4$ (**2a**·$(NO)_2$). Common impurities, which can present difficulties with the synthesis of desired nitrosyl products, include NO_2(g), N_2O_3-(g), and N_2O(g).[4] It can be misleading to assume that NO is the strongest ligand; in fact, NO_2 binds to iron complexes with greater affinity than does NO.[65,75] The addition of purified NO-(g) (see Experimental Section) to a THF solution of [(F_8)Fe^{II}] (**4**) results in the clean formation of [(F_8)Fe(NO)] (**4**·NO), with ν_{NO} = 1684 cm^{-1} (Nujol). Similar vibrational data is reported

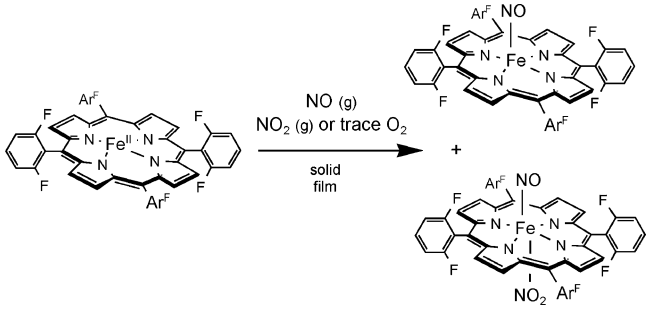

Figure 9. Reaction of [(F_8)Fe^{II}] (**4**) with impure NO(g) results in the in situ formation of the compounds [(F_8)Fe(NO)] (**4**·NO) and [(F_8)Fe^{III}-(NO)(NO_2^-)].

in the literature; a KBr pellet IR spectrum of [(F_8)Fe(NO)] (**4**·NO) exhibits a ν_{NO} = 1687 cm^{-1}.[45] In sharp contrast to these findings, the addition of "unpurified" NO(g) to a thin film of (F_8)Fe^{II} (**4**), which was deposited on a Si−Comp ATR window and held under static vacuum, resulted in the formation of both (F_8)Fe−NO (ν(NO) = 1656 cm^{-1}; $\Delta(^{15}N^{18}O)$ = 68 cm^{-1}) and the nitro-, nitrosyl-complex (F_8)Fe(NO)(NO_2) (ν(NO) = 1868 cm^{-1}; $\Delta(^{15}N^{18}O)$ = 79 cm^{-1} and $\nu_s(NO_2)$ = 1294 cm^{-1}; $\Delta(^{15}N^{18}O)$ = 55 cm^{-1}) (Supporting Information, Figure S9).

It has been suggested that ferrous heme−nitrosyl complexes can promote the disproportionation of NO(g).[64] Our findings suggest that [(F_8)Fe^{II}] (**4**) does not catalyze the disproportionation of nitric oxide to nitrous oxide and nitrogen dioxide (eq 3, below). This result, the first demonstration that an electron-deficient (i.e., with fluorinated F_8 ligand) heme nitrosyl does not promote NO(g) disproportionation, is similar to the findings of Ford and co-workers,[65] who suggest that the more electron-rich (TPP)Fe^{II} systems do not disproportionate NO(g). These researchers suggest that disproportionation products such as [(TPP)Fe(NO)(NO_2)] are formed due to the presence of trace NO_2(g) (e.g., Figure 9).[75]

$$3NO \rightarrow N_2O + NO_2 \qquad (3)$$

It should be noted that the addition of unpurified NO(g) to solid films of [(^{6}L)Fe^{II}···Fe^{II}−Cl]B(C_6F_5)$_4$ (**2a**) resulted in the formation of an intractable mixture of heme−nitrosyl and heme−nitrite complexes, with possible non-heme iron−nitrosyl and non-heme iron−nitrite species. Nonetheless, from within these reaction mixtures it was possible to observe the bands directly related to the compound [(^{6}L)Fe(NO)Fe(NO)−Cl]B-(C_6F_5)$_4$ (**2a**·$(NO)_2$) under most circumstances. Thus, we conclude that there is no NO_x redox chemistry occurring in our heme/non-heme diiron system under the conditions examined with purified NO(g). As already pointed out by Ford,[4,65] our results and observations also show that extreme care must be taken in the purification of NO(g) in order to prevent the observation of anomalous artifacts and non-NO(g)-derived chemistry caused by the presence of trace impurities.

Relevance to NOR and Attempts at Functional Modeling. Purified bacterial NOR has been shown to exist in both an oxidized (e.g. Fe^{III}−O−Fe^{III}) configuration and can be chemically reduced to the diferrous form. The latter has been most often discussed as the "active" enzyme complex capable of nitric oxide reductase activity,[1,2] although some studies suggest that

(71) Pohl, K.; Wieghardt, K.; Nuber, B.; Weiss, J. *J. Chem. Soc., Dalton Trans.* **1987**, 187−192.
(72) Enemark, J. H.; Feltham, R. D. *Coord. Chem. Rev.* **1974**, *13*, 339−406.
(73) Richter-Addo, G. B.; Legzdins, P. *Metal Nitrosyls*; Oxford University Press: New York, 1992.
(74) Scheidt, W. R.; Ellison, M. K. *Acc. Chem. Res.* **1999**, *32*, 350−359.
(75) Kurtikyan, T. S.; Martirosyan, G. G.; Lorkovic, I. M.; Ford, P. C. *J. Am. Chem. Soc.* **2002**, *124*, 10124−10129.

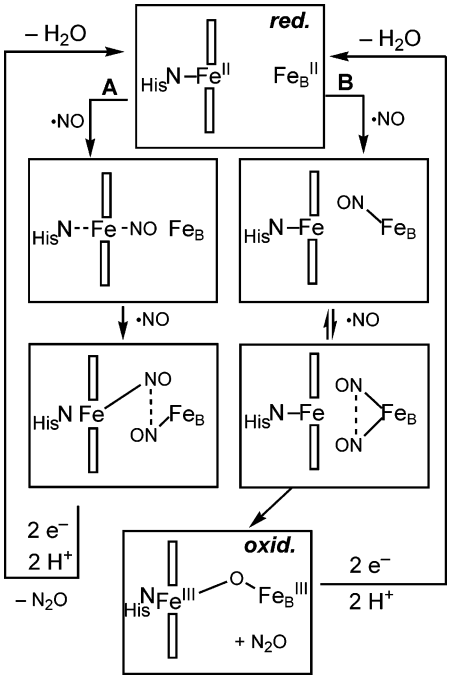

Figure 10. Possible mechanism for the binding of 2 equiv of NO by the NOR enzyme, followed by successive coupling to give nitrous oxide.

a mixed-valent form might also be involved.[76,77] Researchers have also identified both CO- and NO-bound enzyme complexes.[13,16,78] Two possible mechanisms for the binding and reduction of NO at a fully reduced site in NOR are in Figure 10.[2,3,13,22] Route **A** involves the formation of both a heme and non-heme iron−nitrosyl species formed in close proximity to each other. This pathway is supported by the findings that reduced NOR incubated with NO(g) revealed weak EPR signals near $g = 2$ and 4, typical for heme nitrosyl and non-heme iron−nitrosyl species, repsectively.[2,11] As mentioned, [(^{6}L)Fe(NO)-Fe(NO)−Cl]B(C_6F_5)$_4$ (**2a**·$(NO)_2$) does possess an EPR signal at $g \approx 2$. Route **B** involves the formation of a non-heme iron−*cis*-dinitrosyl complex. In either case, there is subsequent reductive coupling of the adjacent nitrosyl ligands to give nitrous oxide. Mechanism **A** does not indicate formation of a μ-oxo species, although such a complex possibly exists at some point during catalytic turnover.[16,22] While NOR is not involved in pumping protons across a cell membrane, protons are integral toward the working of the catalytic cycle. They are needed in breaking the μ-oxo bridge, thereby forming water and, with the addition of two electrons, re-forming the reduced diferrous complex for further NO turnover.

In addition to catalyzing the reduction of nitric oxide to nitrous oxide, NOR has an "oxidase" activity and has been found to catalyze the four electron reduction of dioxygen to water (40 O_2/s),[26,27] thus the possible relevance of our dioxygen chemistry (vide supra). Likewise, cytochrome *c* oxidase (C*c*O) has been shown to catalyze the reduction of NO to N_2O (0.5 NO/s at best).[79−81] While both C*c*O and NOR are capable of catalyzing the same reactions, C*c*O has evolved to efficiently catalyze the reduction of O_2 (250 O_2/s), while NOR remains the most efficient at catalyzing the reductive coupling of NO (200 NO/s).

Much like bacterial NOR, our heme/non-heme diiron complex [(^{6}L)Fe^{II}···Fe^{II}−Cl]$^+$ (**2**) reduces dioxygen and subsequently forms an oxidized Fe^{III}−O−Fe^{III} complex. NOR has been found to bind CO at heme b_3 (ν_{CO} 1970 cm^{-1}).[13,82] Similarly, [(^{6}L)-Fe^{II}(CO)(thf)Fe^{II}−Cl]B(C_6F_5)$_4$ (**2a**·CO) is a low-spin heme−carbonyl species (ν_{CO} 1969 cm^{-1}, film), with the non-heme iron being unreactive toward CO, under the conditions used. Recently, however, the Fe/Fe′ active site of NOR obtained from *Bacillus azotoformans* was found to bind CO at both the heme and non-heme iron sites. Subsequent exposure to increasing concentrations of chloride precluded the formation of a non-heme iron−carbonyl species.[83] This finding suggests that removal of the chloride ligand from the non-heme iron site, in synthetic complexes such as **2**, could lead to a change in chemistry and allow the formation of a non-heme iron−carbonyl. A chloride-free non-heme iron could also possibly have implications for the NO-reductase activity for model systems (vide infra).

The overall goal in the design of the complex [(^{6}L)Fe^{II}···Fe^{II}−Cl]$^+$ (**2**) was as a functional "model" for the reduction of nitric oxide to nitrous oxide, as inspired by bacterial NOR. However, [(^{6}L)Fe(NO)Fe(NO)−Cl]B(C_6F_5)$_4$ (**2a**·$(NO)_2$) is thermally stable and does not seem to react further to give nitrous oxide upon the addition of proton sources. By analogy to the putative mechanism for NOR-mediated NO reduction, we also investigated the effects of adding axial ligands to [(^{6}L)Fe(NO)-Fe(NO)−Cl]B(C_6F_5)$_4$ (**2a**·$(NO)_2$) in an effort to drive N−N reductive coupling. Unfortunately, the addition of an excess of 1,5-dicyclohexylimidazole or (dimethylamino)pyridine to THF solutions of [(^{6}L)Fe(NO)Fe(NO)−Cl]B(C_6F_5)$_4$ (**2a**·$(NO)_2$) resulted in the isolation of the reduced complex [(^{6}L)Fe^{II}···Fe^{II}−(Cl)]$^+$ (**2**) (eq 4), as confirmed by UV−visible and FTIR spectroscopies.

$$\underset{\mathbf{2}\cdot(NO)_2}{Fe^{II}-(NO)_2-Fe^{II}} + \text{excess "base"} \rightarrow \underset{\mathbf{2}}{Fe^{II}\cdots Fe^{II}} + 2NO(g) \quad (4)$$

The evolution of nitric oxide from these systems was observed using both gas chromatography (NO detected by TCD) and by trapping with the complex [(F_8)Fe^{II}] (**4**) (yielding (F_8)Fe^{II}−NO by UV−visible spectroscopy). Ligand-promoted nitric oxide dissociation from ferrous heme nitrosyl complexes has previously been reported,[45] suggesting that our system is thermodynamically driven to release NO (as free NO and not NO^-, the latter of which could drive N−N coupling) upon the addition of excess axial ligands.

Additional attempts to drive N−N coupling, or to otherwise effect NO disproportionation, were also unsuccessful. Further, [(^{6}L)Fe(NO)Fe(NO)−Cl]B(C_6F_5)$_4$ (**2a**·$(NO)_2$) was stable in the presence of excess nitric oxide. Attempts to form a dinitrosyl exclusively at the non-heme iron site, to possibly induce

(76) Gronberg, K. L. C.; Roldan, M. D.; Prior, L.; Butland, G.; Cheesman, M. R.; Richardson, D. J.; Spiro, S.; Thomson, A. J.; Watmough, N. J. *Biochemistry* **1999**, *38*, 13780−13786.
(77) Groenberg, K. L. C.; Watmough, N. J.; Thomson, A. J.; Richardson, D. J.; Field, S. J. *J. Biol. Chem.* **2004**, *17*, 17120−17125.
(78) Cheesman, M. R.; Zumft, W. G.; Thomson, A. J. *Biochemistry* **1998**, *37*, 3994−4000.
(79) Brudvig, G. W. S., T. H.; Chan, S. I. *Biochemistry* **1980**, *19*, 5275−5285.
(80) Brunori, M. *Trends Biochem. Sci.* **2001**, *26*, 21−23.
(81) Giuffre, A.; Stubauer, G.; Sarti, P.; Brunori, M.; Zumft, W. G.; Buse, G.; Soulimane, T. *Proc. Natl. Acad. Sci. U.S.A.* **1999**, *96*, 14718−14723.
(82) Matsuda, Y.; Uchida, T.; Hori, H.; Kitagawa, T.; Arata, H. *Biochim. Biophys. Acta* **2004**, *1656*, 37−45.
(83) Lu, S.; Suharti; de Vries, S.; Moënne-Loccoz, P. *J. Am. Chem. Soc.* **2004**, *126*, 15332−15333.

coupling, were also unsuccessful. In such reactions, a silver pseudohalide (e.g., AgOTf, $AgSbF_6$) was added prior to the introduction of NO to frozen solutions of $[(^6L)Fe^{II}\cdots Fe^{II}-(Cl)]^+$ (**2**), hoping to remove the non-heme chloride ligand in situ, thereby creating a vacant labile site and enhancing reactivity. But, these reactions failed to yield the desired nitrous oxide product. As mentioned, the current mechanism postulated for the reductive coupling of NO to give N_2O by NOR is "catalysis by approximation". According to this view, adjacent iron−nitrosyls have sufficient driving force to couple (with additional donated electrons) and yield N_2O. The fact that we could not drive the coupling of adjacent stable iron−nitrosyls suggests that the putative biological mechanism may be overly simplified, and that other reaction mechanisms need to be contemplated and tested. Planned second-generation model systems might benefit by (1) incorporating an intramolecularly tethered axial base and (2) altering the non-heme iron site ligand donor set, including that it be chloride free.

Summary/Conclusions

The heme/non-heme diiron active site of NOR is a (quite) new prosthetic group active site entity in bioinorganic enzymology. The first synthetic model for the reduced diiron center is presented here, along with biologically relevant chemical reactivity including interactions with O_2, CO and NO gases.

The dioxygen adducts and dioxygen reduction chemistry observed functionally models the NOR O_2 chemistry, as $[(^6L)Fe^{II}\cdots Fe^{II}-(Cl)]^+$ (**2**) readily reacts with 1/2 O_2 to give the "resting" or oxidized species $[(^6L)Fe^{III}-O-Fe^{III}-Cl]^+$ (**1**). This two-electron reduction of dioxygen to an oxo (O_2^{-}) product involves the initial formation of a heme−superoxo species which was detected at low temperature by both UV−visible and RR spectroscopies. This represents the first direct detection of a heme−superoxo intermediate in heme/non-heme diiron chemistry en route to the formation of a μ-oxo bridge heme/non-heme complex. The inevitable fate of the heme−superoxo complex is the thermal decay by disproportionation (and evolution of 1/2 O_2) to give the μ-oxo complex $[(^6L)Fe^{III}-O-Fe^{III}-Cl]^+$ (**1**). We suggest that an iron−peroxo−iron species, of an inter- or intramolecular nature, likely exists as a short-lived intermediate en route to oxo formation.

Similarly, the CO and NO reactivity of coordination compounds inspired by the reduced NOR active site has been developed. $[(^6L)Fe^{II}\cdots Fe^{II}-(Cl)]^+$ (**2**) reacts with CO(g) or NO(g) to give a stable monocarbonyl species $[(^6L)Fe(CO)Fe-Cl]^+$ (**2**·CO) or dinitrosyl species $[(^6L)Fe(NO)Fe(NO)-Cl]^+$ (**2**·$(NO)_2$), respectively. Unfortunately, from the standpoint of nitric oxide reduction, the intrinsic heme−NO and (TMPA)Fe−NO functionalities (i.e., one heme; one non-heme) are both stable when tethered (i.e., here in **2**·$(NO)_2$) or otherwise exposed to each other. Further efforts in our laboratory are aimed at functional modeling of NOR via the design and study of new ligand systems for heme/non-heme diiron chemistry.

Acknowledgment. This work was supported by National Institutes of Health Grants GM60353 (to K.D.K.) and GM18865 (to P.M.-L.).

Supporting Information Available: High-frequency RR spectra for the reaction of dioxygen with **2** (Figure S1), high-frequency RR spectra for the reaction of dioxygen with the empty tether complex $[(^6L)Fe^{II}]$ (**3**) in THF (Figure S2), FTIR spectrum for **2a**·CO (Figure S3), ^1H NMR spectrum for **2a**·CO (Figure S4), MALDI-TOF-MS for **2**·$(NO)_2$ (Figure S5), ^1H NMR spectrum of **2**·$(NO)_2$ (Figure S6), in situ RIR monitoring of the reaction of solid films of **2a** with NO(g) (Figure S7) and solid films of $[(^6L)Fe^{II}]$ (**3**) with NO(g) (Figure S8), and the FTIR difference spectra for $[(F_8)Fe]$ (**4**) + unpurified $^{14}NO/^{15}NO$ (Figure S9). This material is available free of charge via the Internet at http://pubs.acs.org.

JA0458773